Mapping the Binding Site of Melanocortin 4 Receptor Agonists: A Hydrophobic Pocket Formed by I3.28(125), I3.32(129), and I7.42(291) Is Critical for Receptor Activation

Kristine Hogan,[†,⊥] Stephan Peluso,[‡,▽] Sandy Gould,[‡] Ian Parsons,[§] Dominic Ryan,[∥] Lijun Wu,[†,⊗] and Irache Visiers*[,∥]

Departments of Molecular and Cellular Pharmacology, Medicinal Chemistry & Metabolic Diseases, Analytical Chemistry, and Computational Chemistry, Millennium Pharmaceuticals, Cambridge, Massachusetts 02446

Received August 8, 2005

The melanocortin 4 receptor is involved in the control of the feeding behavior and energy homeostasis. It is regulated by internal agonist (α-MSH) and antagonists (Agouti). Peptide agonists bind in a β-turn conformation that organizes the characteristic message sequence (His-L/DPhe-Arg-Trp) in an optimal arrangement for binding and activation of the receptor. Our goal is to determine the most likely binding modes of peptide and small molecule agonists to use this information to guide our structure-based drug design efforts. Previous studies have identified some residues that are likely to be involved in peptide agonist binding, giving an initial estimate of the main contacts between peptides and receptor. However, a more detailed description of the orientation of the peptide in a β-turn conformation in the binding site, as well as of the small molecule agonists, and it is commonalities with the peptide agonist binding modes is necessary to serve as the basis for structure-based drug design. In the current study we combine site-directed mutagenesis with molecular modeling studies to determine the most likely binding mode of peptide and small molecule agonists, and we found that Y6.58(268), Y7.38(287), I3.28(125), I3.32(129), and I7.42(291) also line the binding site and are likely to have direct contacts with the MC4R agonists. Of particular interest are residues I3.28(125), I3.32(129), and I7.42(291), which form a hydrophobic pocket where I7.42(291), on top of the NPXXY motif, is likely to act as a new rotamer switch implicated in the activation of the receptor.

Introduction

The melanocortin 4 receptor (MC4R) belongs to the rhodopsin-like G-protein-coupled receptor (GPCR) family, characterized by a scaffold of seven transmembrane segments (TM) connected by extracellular and intracellular loops. It is exclusively expressed in the brain and is involved in the control of the feeding behavior and of energy homeostasis.[1] Mutations in the MC4R are associated with congenital obesity.[2−5] Agonists of the MC4R cause a reduction of food intake by inducing satiety,[6] while antagonists promote feeding.[7] The involvement of the MC4R in feeding disorders makes it an attractive pharmaceutical target in the development of drugs to the treatment of obesity and other eating disorders.

The endogenous agonists for the melanocortin receptors are derived from pro-opiomelanocortin (POMC) which after post-translational cleavage generates α and γ melanocyte stimulating hormones (MSH) and adrenocorticotropin (ACTH). α-MSH is a linear peptide with 13 residues (Ac−Ser-Tyr-Ser-Met-Glu-His-Phe-Arg-Trp-Gly-Lys-Pro-Val-NH_2). Substitution of Phe-7 and Met-4 for D-Phe and norleucine respectively yields NDP-α-MSH, which is more potent than α-MSH. Interestingly, all melanocortin peptide agonists contain a His-(L/D)Phe-Arg-Trp consensus sequence that is considered the "message" sequence, responsible for selectivity and activation of the melanocortin receptors.[8] The bioactive conformation of agonists peptides involves a β-turn on the His-(L/D)Phe-Arg-Trp motif[9,10] which is likely to serve as an organizing scaffold to orient the side chains of the message sequence in the best orientation for interaction with the receptor. This hypothesis has been supported by the recent discovery of turn-mimetics with MC4R agonist character.[11] In addition to agonists with peptidic or peptidomimetic character, a number of nonpeptidic agonists have been developed, including compound **3** (also published as THIQ) and compound **4** (Figure 1).[12,13]

AGONISTS:
NDP-α−MSH:
Ac-Ser-Tyr-Ser-Nle-Glu-His-Dphe-Arg-Trp-Gly-Lys-Pro-Val-NH2
α-MSH:
Ac-Ser-Tyr-Ser-Met-Glu-His-Phe-Arg-Trp-Gly-Lys-Pro-Val-NH2
Peptide 1:
c[Ser-Tyr-Thr-His-DPhe-Arg-Trp-Thr-Ile-Pro]

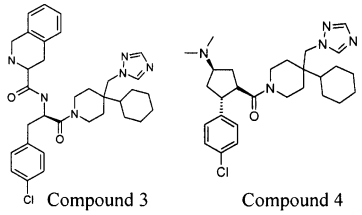

Compound 3 Compound 4

ANTAGONISTS:
AGRP(83-132):
SSRRCVRLHESCLGQQVPCCDPCATCYCRFFNAFCYCRKLGTA MNPCSRT
Peptide 2:
c[Thr-Tyr-Thr-His-DNaf-Arg-Trp-Thr-Ile-DPro]
Compound 5 (ML00253764):

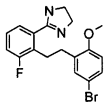

Figure 1. Ligands used in the study.

In the absence of a crystal structure of the MC4R, free or in complex with a ligand, little is known about the exact orientation

* To whom correspondence should be addressed: 40 Landsdowne Street, Cambridge, MA 02446. Phone: 001-617-444-1367. Fax: 617-551-8907. E-mail: visiers@mpi.com.
† Department of Molecular and Cellular Pharmacology.
‡ Department of Medicinal Chemistry & Metabolic Diseases.
§ Department of Analytical Chemistry.
∥ Department of Computational Chemistry.
⊥ Current address: MIT Lincoln Labs, Lexington, MA 02420.
⊗ Current address: Novartis Institutes for Biomedical Research, Cambridge, MA 02139.
▽ Current address: Infinity Pharmaceuticals, Cambridge, MA 02139.

10.1021/jm050780s CCC: $33.50
Published on Web 01/12/2006

Table 1. Ideal and Actual Backbone Angles Characterizing the His-DPhe-Arg-Trp Sequence for Decapeptide "Peptide **1**" (Figure 1)

	Φ i+1	Ψ i+1	Φ i+2	Ψ i+2
ideal type II′	60 ± 30	−120 ± 30	−80 ± 30	60 ± 30
NMR selected structure	65.8	−91.6	−138	27.9

of MC4 agonists in their binding pocket. Homology models of GPCRs based on bovine rhodopsin in combination with site-directed mutagenesis have been successfully used in the past to provide a structural framework for both ligand binding and functional studies; examples of these are the serotonergic,[14] opioid,[15] adrenergic,[16] dopaminergic,[17] and gonadotropin releasing hormone receptors[18] among others. Previous studies using homology models together with structure−activity relationships of peptide agonists, have determined some of the amino acids that are likely to be part of the binding site of MC4R, mainly D3.25(122), D3.29(126) in TM3,[19,20] E100(2.60) in TM2,[21] and F6.52(262) in TM6.[8] However a more detailed description of the precise orientation of the peptides and small molecule ligands in the binding site is lacking and is critical for structure-based drug design purposes. In this study we have developed a model of the MC4R that incorporates the conformational changes that occur upon receptor activation and are likely to affect the shape of the binding site. This model was used to dock a peptide with the His-(L/D)Phe-Arg-Trp consensus sequence locked in a β-turn conformation, as well as a few agonist ligands. The most likely binding poses suggested that in addition to the residues reported in the literature, Y6.58(268), Y7.38(287), I3.28(125), I3.32(129), and I7.42(291) line also the binding site of MC4R agonists. Site-directed mutagenesis was used to test the relevance of these residues in ligand binding and activity. These studies support the proposed binding mode and lead to the identification of a new hydrophobic and aliphatic pocket formed by I3.28-(125), I3.32(129), and I7.42(291), which plays a crucial role in the transmission of the activation signal.

We have generated a consistent three-dimensional geometric arrangement of the pharmacophoric elements for peptide and small molecule MC4R agonists. The results shown in this study provide a solid background for structure-based drug design efforts by identifying the nature of the key interactions between the MC4R and its agonists.

Experimental Section

Ligands Used in the Study. The ligands presented in this study are shown in Figure 1. NDP-α-MSH and α-MSH were purchased from Sigma (St Louis, MO). Radiolabeled [^{125}I] NDP-α-MSH was obtained from Amersham Biosciences, Corp. (Piscataway, NJ). Compounds **3** and **4** were prepared according to the procedure described in the literature.[12,13,22] AGRP 83-132 was obtained from Phoenix Pharmaceuticals, Inc. (Belmont, CA). Compound **5** (previously reported as compound ML00253764) was obtained as described previously.[23]

Cyclic decapeptides **1** and **2** have been designed to feature the MC4 consensus tetrapeptide sequence His-DPhe/DNal-Arg-Trp locked in a β-turn type II′ conformation. A β-turn is defined for four consecutive residues (denoted by i, i+1, i+2, and i+3) if the distance between the C-alpha atom of residue i and the C-alpha atom of residue i+3 is less than 7 Å and if the central two residues are not helical. Each type of turn is classified according to the Φ and Ψ angles; Table 1 shows the ideal values for a type II′ β-turn.[24] The design we used for these peptides was based on the Schwyzer−Hodges principle[25] which suggests that cyclic peptides containing $2(2n + 1)$ residues (i.e. 6, 10, 14...) would form two β-hairpin under the condition that they contain two equally separated β-turns. Several cyclic peptides responding to this rule of thumb have been shown to adopt a stable β-sheet conformation by NMR and X-ray structure determination.[25−27] The type of β-turn adopted by a particular sequence is related to its amino acid content. In particular type II′ β-turns are known to have a strong preference (76%) for glycine or D-amino acids in the i+1 position.[28] Accordingly, cyclic decapeptides **1** and **2** include two β-turn type II′ inducer sequences His-DPhe/DNal-Arg-Trp and Ile-DPro-Ser-Tyr[29] linked by threonines. The threonine linker was chosen for its propensity to appear in interstrand residue pairs where it usually adopts sterically favored X1 conformations, which facilitates intrapair hydrogen bonding interactions[30,31] (Figure 2).

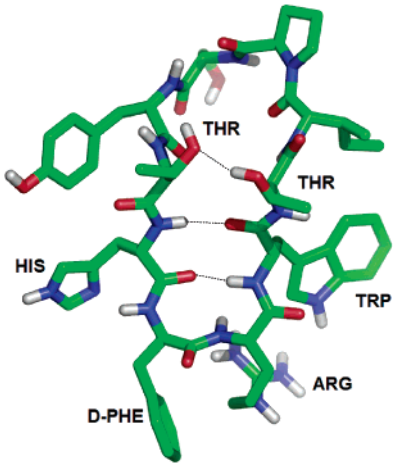

Figure 2. NMR conformation of peptide **1** showing the hydrogen bonds stabilizing the β-turn.

Linear sequences of the decapeptides were assembled on SASRIN resin following Fmoc/tBu protocols and released by repeated treatment with TFA/DCM 1:99. Side chain protected peptides were cyclized under high dilution conditions in DMF using HATU/collidine as activating reagents, deprotected by treatment with TFA/DCM/H_2O/TIS 95/5/2.5/2.5, and then purified by HPLC.

NMR structure determination of these two cyclic peptides was performed in DMSO-d_6 at 600 MHz. Two-dimensional TOCSY and NOESY NMR data enabled ^{1}H signals to be assigned. DQ-COSY and the NOESY data with a mixing time of 120 ms were used in order to generate distance and dihedral angle restraints, through analysis in Felix software (Accelrys). These constraints were divided into categories of "strong", "medium", and "weak" interactions, based on the volume integral of the corresponding NOESY cross-peak, relative to those of the fixed geminal H-β protons of the Ser and Trp residues. A family of 60 structures of the c-[Ser-Tyr-Thr-His-DPhe-Arg-Trp-Thr-Ile-DPro] peptide was derived by distance geometry followed by a simulated annealing protocol, from the NOE restraints, using the NMR refine module of Insight-II software package (Accelrys). The backbone RMSD of these 60 structures around the His-D-Phe-Arg-Trp residues was measured as 0.92 Å. After discarding 14 outliers from the 60 structures, backbone alignment of the remaining 46 structures gave a backbone RMSD around the His-D-Phe-Arg-Trp sequence of 0.68 Å. One of these structures was used as an initial input in the docking study with the MC4 receptor. The NMR and distance geometry analysis showed that both designed peptides average around the expected cyclic β-hairpin conformation encompassed by two β-turns of type II′.

Residue Numbering Scheme. Residues are numbered using the general numbering scheme proposed by Ballesteros and Weinstein.[32] The scheme is composed of a number identifying the transmembrane segment (1 to 7), and a number relative to the most conserved residue in the TM segment, which is assigned number 50; the rest of the residues are numbered relative to this most conserved residue with numbers decreasing toward the N terminus and increasing toward the C-terminus. We also include in parentheses the sequence number for each particular residue (e.g. I3.28(125)).

Molecular Model of the MC4R. A model of the MC4 receptor was constructed using the 2.8 Å resolution crystal structure of

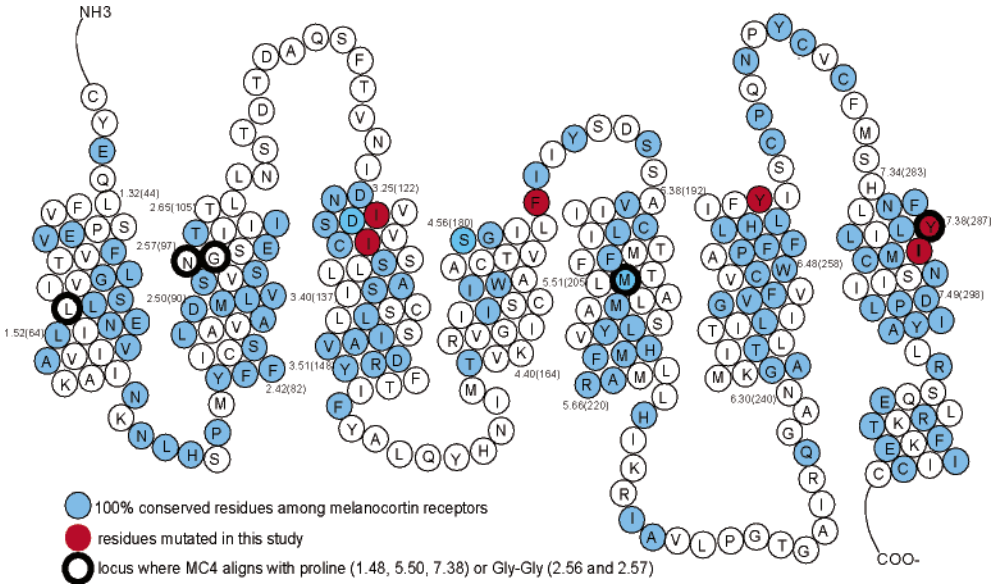

Figure 3. Helical net of the hMC4R. Highlighted in red are the residues we have mutated in this study. A thick line marks positions where the sequences of MC4 and rhodopsin differ in the presence or absence of a proline residue.

rhodopsin as initial template[33] following the criteria and procedures published earlier.[34] A set of 10 intermediate homology models were built; each intermediate was minimized to an energy gradient of 0.01 kcal, and the intermediate model with the best packing quality was selected (MOE, Chemical Computing Group, Inc). Further refinement consisted of the reduction of the kinks in TM1 (locus 1.48), TM2 (locus 2.56/2.57), TM5 (locus 5.50), and TM7 (locus 7.38) as a consequence of the presence of proline or Gly-Gly in the rhodopsin structure, used as a template; given the absence of proline or glycine at these or contiguous locations in the MC4R (Figure 3), we inferred that the MC4R was not likely to present such distortions.[34] The geometry of proline kinks is defined by three parameters, bend angle, wobble angle, and face shift, and can be measured with the program Prokink published earlier[35] (free download at http://icbtools.med.cornell.edu/prokink/). Concisely, the bend angle measures the angle between the helix segments preceding and following the proline; wobble angle describes the orientation of the kink in the three-dimensional space, and the face-shift determines whether the proline local distortion corresponds to a hyper-wound helix (3−10 helix, standard value = −26.4) or to an unwound one (π-helix, standard value = 49.5). The reference values for an ideal α-helix are bend = 0−1, face-shift = 13. The kinks induced by P1.48, P5.50, and P7.38 in rhodopsin are characterized by bend angles of 11.7, 14.2, and 8.6, respectively. Larger departures from the standard α-helical values are observed for the wobble angle and face-shift: P1.48 has a wobble angle = −134.6 and a face-shift = 41.9; P5.50 has a wobble = −169.1 and face-shift = 62.3; P7.38 shows a wobble angle = −165.3 and a face-shift = 36.3. The three prolines are thus preceded by a turn of a helix with face-shift values closer to a π helix and are therefore slightly unwound. We changed the Φ and Ψ dihedral angles of residues i (position aligned with proline in rhodopsin) to i−4 to the standard values of an α-helix (Φ = −58, Ψ = −47). In every case the cytoplasmic end of the helix was kept fixed initially, while allowing changes on the most extracellular segment. Before proceeding to optimize the model obtained by straightening TM1, TM2, TM5, and the N-terminus of TM7, additional fine-tuning was necessary to prepare the protein model for the docking of agonists which have higher affinity for the activated state of the receptor.[36,37] On the basis of abundant literature data, receptor activation involves: i) a clockwise rotation and movement of the cytoplasmic end of TM6 apart from TM3 (viewed from the intracellular side),[38−40] ii) a reduction in the distance between the cytoplasmic ends of TM5 and TM6,[41] and iii) a switch in the orientation of W6.48 from perpendicular to parallel to the plane of the membrane[42] associated with a concerted change in the conformation of the aromatic cluster of residues in TM6 (F6.44(254), W6.48(258), and F6.52(262)).[43] Thus, we first changed the conformation of F6.44-(254), W6.48(258), and F6.52(262), and second we reduced the kink induced by P6.50(260) in TM6 from an initial 30° to a final, lower kink of 11°.

These manual adjustments in the TM kinks generated clashes among helices which needed to be alleviated by rigid body repositioning of the modified helices. Such reorientation was performed so that i) the three-dimensional disposition of key structural motifs part of the rhodopsin family fingerprint was preserved (unless intentionally changed as described above), ii) conserved residues on the modified TM1, TM5, TM6, and TM7 faced the interior of the bundle, and iii) good packing between contiguous helices was achieved. The obtained model was energy minimized with the CHARMM force field[44] using a distance dependent dielectric constant to an energy gradient of 0.01 kcal.

Ligand Orientation in Molecular Models of Receptor Complexes. We selected one of the NMR conformations of peptide **1** and docked the His-DPhe-Arg-Trp fragment derived from this conformer into the receptor as described below. This decapeptide conformation (Figure 2) showed some of the characteristic hydrogen bonds of an antiparallel beta-sheet and the dihedral angles for the turn formed by the His-DPhe-Arg-Trp tetrapeptide consensus sequence were close to a type II′ β-turn (Table 1).

The conformations of compounds **3** and **4** used as starting point for our docking studies were obtained by simple energy minimization. These minimized structures were characterized by an axial orientation of the cyclohexane attached to the piperidine ring, which was corroborated by the NMR analysis of their solution structures (data not shown). Even though the conformation in the complex may differ from that in solution, it was considered a reasonable initial conformation for the flexible docking studies.

The docking of the ligands was performed with qxp+, using the fulldock+ algorithm[45] with one of D3.29(126) oxygens as center of the binding site. The side chains of residues which are presumed to be directly involved in ligand binding were allowed to move (E2.60(100), D3.25(122), D3.29(126), Y187, C5.42(196), M5.46-(200), F5.47(201), F6.44(254), W6.48(258), F6.51(261), F6.52(262), H6.54(264), L6.55(265), Y7.38(287)). The tetrapeptide was constrained in its β-turn conformation by distance constrains between the backbone atoms forming the β-turn. The same types of constraints were also applied to the backbone atoms of residues involved in intramolecular hydrogen bonds to preserve the integrity of such bonds during the simulation. Compounds **3** and **4** were allowed complete flexibility during the docking run. Fifty poses

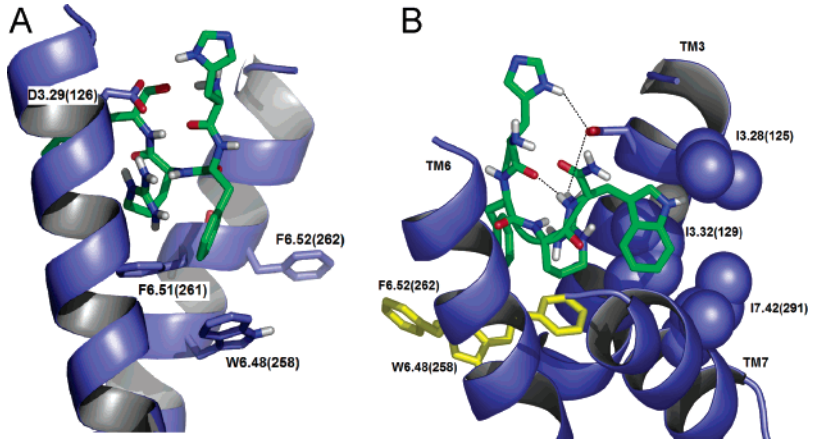

Figure 4. Proposed binding mode for the core agonist sequence "His-DPhe-Arg-Trp". Both pictures A and B show the same binding pose from two different angles. A: Orientation showing i) an aromatic interaction between the DPhe and an aromatic cluster of residues in TM6 including F6.52(262), F6.51(261), and W6.48(258); ii) hydrogen bond of D3.29(126) with His and Arg of the core agonist peptide. B: Same pose as A, different orientation showing the ligand Trp fitting in a hydrophobic pocket formed by I3.28(125), I3.32(129), and I7.42(291).

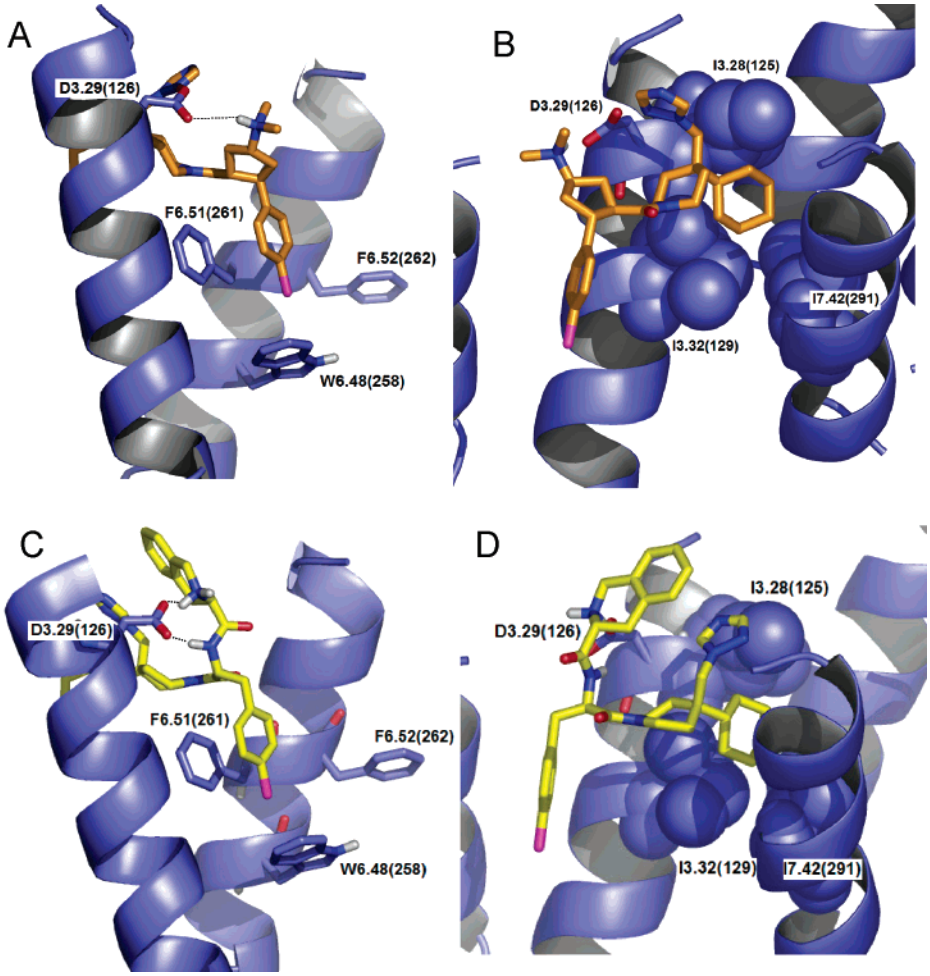

Figure 5. Two views of preferred pose of compound **4** (A and B) and compound **3** (C and D). A, C: Orientation showing an aromatic interaction between the chlorophenyl ring of the agonist and the aromatic cluster of residues in TM6 comprising residues F6.51(261), F6.52(262), and W6.48-(258). The interaction between the positive amine and D3.29(126) can also be seen. B, D: Orientation showing the position of the cyclohexane of compounds **4** and **3** in the hydrophobic pocket formed by I3.28(125), I3.32(129), and I7.42(291). The interaction of D3.29(126) with the positive amine and the imidazole ring of compounds **4** and **3**, is also apparent.

were saved for each run, which were filtered in agreement to published mutagenesis data mainly: i) an ionic interaction with D3.29(126) in TM3,[21,46] ii) a hydrophobic interaction with F6.52-(262),[8] iii) for the peptides, a Zn^{2+}-mediated interaction between His7 and D3.29(126) or D3.25(122) should be possible.[19,20] One pose was selected for the tetrapeptide (Figure 4) and two possible poses for each one of the small molecule agonists, compound **3** and **4** (Figure 5).

Reagents. All primers were synthesized and HPLC purified by Sigma-Genosys (The Woodlands, TX). All cell culture reagents were from Invitrogen Life Technologies (Carslbad, CA) except for fetal calf serum which was obtained from HyClone (Logan, UT).

Receptor Mutagenesis. Human MC4 receptor cDNA was cloned into pIRES-puro (Clontech Laboratories, Palo Alto, CA) containing an in-frame myc-tag at the n-terminus. The construct was then used for subsequent mutant generation. To introduce point mutations a two-stage polymerase chain reaction (PCR) using *Pfu* polymerase (Stratagene, La Jolla, CA) was used. Internal primers containing the desired mutations were designed to be complementary to each other for at least 15 nucleotides at their 5′ ends. External forward and reverse primers were designed to anneal outside the coding region of pIRES-puro. All reactions were carried out using the following cycling parameters: 95 °C for 30 s, 55 °C for 1 min and 72 °C for 2 min for a total of 30 cycles. The first stage PCR amplifications were performed in two separate reactions, with one internal and one external primers to produce the 5′ and 3′ fragments of the desired final PCR product. These two fragments were treated with *Dpn* I to digest template DNA and then purified by agarose gel electrophoresis. The fragments were then used as template for the second stage PCR amplification with external primers to produce full-length MC4R mutants. All PCR products were cloned into pIRES-puro containing an in-frame myc-tag at the N-terminus. Mutant MC4 receptor sequences were confirmed by DNA sequencing.

Cell Culture and Transient Transfection. HEK-293 cells were maintained in DMEM with 10% fetal calf serum in a humidified 5% CO_2/95% air atmosphere. The day before transfection cells were seeded at 5×10^6 cells/100-mm dish. Seven micrograms of mutant or wild-type DNA was transfected using FuGENE−6 (Roche Diagnostics, Indianapolis, IN) according to the manufacturer's protocol. Cells were incubated for a total of 48 h prior to being used in bioassays.

Binding Assays. Whole cell binding assays were performed on HEK-293 cells transiently transfected with MC4 receptor constructs. 48 h post transfection cells were lifted with 0.5 mM EDTA washed several times in binding buffer [(25 mM HEPES, 1.5 mM $CaCl_2$, 1 mM $MgSO_4$, 0.1 M NaCl, 0.5% BSA, 1 mM 1,10 phenanthroline, and one complete EDTA-free protease inhibitor tablet (Roche Diagnostics, Indianapolis, IN)/100 mL) pH 7]. Cells were then incubated in a total volume of 100 μL for 3 h with 0.25 nM ^{125}I NDP-α-MSH and various concentrations of nonradiolabeled ligands or compounds. In the case of Y7.38(287)A, 1 nM of radiolabeled NDP was used. For saturation experiments a range of 0.0025 to 5 nM of ^{125}I NDP-α-MSH, and 3 μM of nonradiolabeled NDP-α-MSH (nonspecific) or buffer (total) were used. The reaction was terminated by rapid filtration using a vacuum harvester with ice-cold wash buffer [(25 mM HEPES, 1.5 mM $CaCl_2$, 1 mM $MgSO_4$, 0.5 M NaCl) pH 7]. The filters were allowed to dry and 50 μL/well scintillation fluid was added. The amount of radioactivity present was determined by scintillation counting on Microbeta Trilux (Wallac, Boston, MA). Each experiment was performed 2−3 times with duplicate wells. To determine specific binding, nonspecifically bound radioactivity was subtracted from total bound activity. Binding displacement curves were drawn using Prism (GraphPad Software, San Diego, CA). The maximum binding (B_{max}) was calculated using the equation B_{max} = [NDP-α-MSH specific binding]/([NDP-α-MSH]/(K_d + [NDP-α-MSH]). $K_i = IC_{50}/(1+$ [NDP-α-MSH]/K_d). Empty vector transfected cells did not show any specific binding to ^{125}I NDP-α-MSH.

Cyclic AMP Assays. HEK-293 cells transiently expressing mutant or wild-type receptor were generated as described above. Cells were lifted at 24 h with Trypsin/EDTA and plated into 96-well polylysine coated plates (0.6×10^5 cells/well). Forty eight hours post transfection the supernatant was removed and the cells were preincubated for 10 min in Opti-MEM (Invitrogen Life Technologies, Carslbad, CA) containing 0.5 mM isobutylmethylxanthine. They were then stimulated with various concentrations of ligands or compounds for 30 min at 37 °C. Cells were then lysed, and cAMP accumulation was measured using Tropix cAMP−Screen 96-well cAMP Immunoassay System (Applied Biosystems, Foster City, CA) according to the manufacturer's protocol. For the antagonist assay compound was preincubated with cells for 15 min prior to addition of NDP-α-MSH at EC_{50} concentration. Each experiment was performed a minimum of three times with duplicate wells.

Results

The structures and names of the ligands used are shown in Figure 1.

1. Ligand Orientation in the MC4R Molecular Model. To explore the common features between the peptide agonists and small molecule agonists, as well as the molecular determinants of their agonist character, we have investigated the most likely binding mode of compounds **3** and **4** as well as a tetrapeptide consisting of the core sequence His-DPhe-Arg-Trp as described under Experimental Section. We found that only one of the main poses obtained for the tetrapeptide showed the interactions reported previously in the literature,[8,19−21,46] while preserving the antiparallel beta-sheet and β-turn character. This pose was characterized by an aromatic interaction between D-phenylalanine and an aromatic cluster of residues in TM6 in addition to a double electrostatic interaction between two amino acids from the peptide (arginine and histidine) with D3.29(126) (Figure 4) in the receptor. Besides these interactions, this pose was characterized by a contact between tryptophan and a hydrophobic cluster of residues including I3.28(125), I3.32(129) and I7.42(291), and Y7.38(287) (Figure 4B).

The docking runs for the nonpeptidic agonists compounds **3** and **4** yielded two main binding poses. The first pose was characterized by a hydrogen bond between Y7.38(287) and the carbonyl of the ligands; this hydrogen bond was absent in the second main pose, which penetrated deeper into the bundle, positioning the chloroaryl ring close to the aromatic cluster in TM6 (Figure 5A and 5C), and the cyclohexane ring in the cavity formed by I3.28(125), I3.32(129), and I7.42(291) (Figure 5B and 5D). Both poses included an ionic interaction with D3.29-(126) and a hydrophobic interaction with the aromatic cluster in TM6; the triazole moiety was close to the aromatic cluster in TM6 in the first pose, while the second pose oriented it toward the extracellular loops, possibly interacting with water and/or the conserved aspartate D3.29(126) (Figure 5). On the basis of our docking studies, we also predicted that residue Y6.58(268) faces the interior of the bundle, very close to the extracellular loops. The larger peptide agonists extend higher than compound **4** up in the binding site and were predicted to have more significant contacts with Y6.58(268) (Figure 6).

2. Site-Directed Mutagenesis. Site-directed mutagenesis experiments were used to test the hypothesis proposed by analysis of the results of the docking simulations of the compounds shown in Figure 1. The selected docking poses suggested that, in addition to the previously published amino acids, residues Y6.58(268), Y7.38(287), I3.28(125), I3.32(129), and I7.42(291) are also likely to line the binding site of the MC4R agonists, providing key contacts for both peptide and small molecule agonists. To test the validity of our ligand binding hypothesis, we have studied the impact of the mutation of each delineated residue on ligand binding and functional activity and on the basal activity of the receptor. The selected mutant constructs were designed to test specific hypothesis regarding the nature of the physical interaction of each particular locus with the ligand. Residues Y6.58(268) and Y7.38(287) were mutated to phenylalanine and alanine, respectively. The Y/F mutation allowed us to examine the importance of the hydrogen bonding capability of tyrosine on the function of the receptor and/or ligand potency, while maintaining the aromatic character of the residue. The Y/A mutation was designed to reduce the volume and hydrophobicity of the residue at that position.

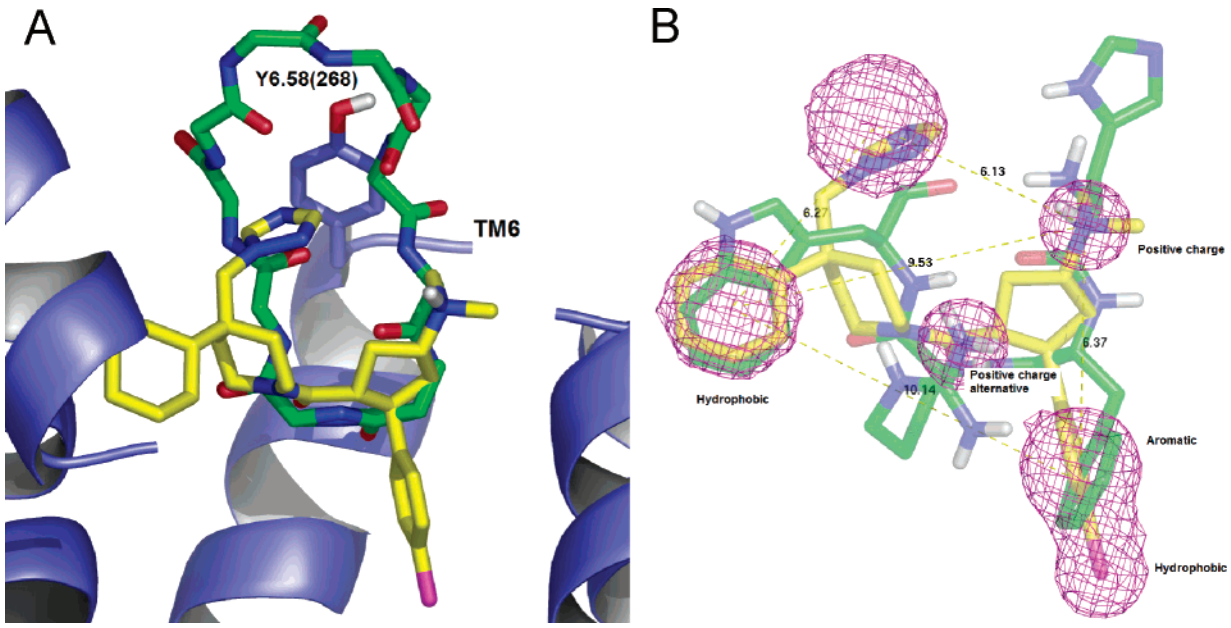

Figure 6. (A) Overlap of the preferred binding pose of compound **4** and the backbone of the representative NMR structure of the cyclic decapeptide **1** used to define the conformation of the His-DPhe-Arg-Trp consensus sequence used in the docking studies. The larger peptide extends toward the extracellular part of the bundle, higher than compound **4**, and therefore has more significant contacts with Y6.58(168). (B) Overlap of the preferred binding pose of compound **4** and the His-DPhe-Arg-Trp motif on the proposed pharmacophore. The position of the positive nitrogen is variable as described in the discussion section, and therefore the distances involving this nitrogen as shown here correspond only to the particular molecule shown in the figure.

As mentioned earlier, our docking studies showed that isoleucines I3.28(125), I3.32(129), and I7.42(291) (Figures 4B, 5B and 5D) form a hydrophobic aliphatic pocket where the cyclohexane of nonpeptidic agonists and the tryptophan of peptide agonists were likely to interact. Each isoleucine was mutated to alanine, one at a time, thus reducing the size of the residue at this position, while keeping a hydrophobic residue. Last, we mutated F4.60(184). This last residue is the first residue of the second extracellular loop and is therefore positioned in a flexible area; our model suggested that this residue might participate in the binding site. To explore the role of this residue, we mutated it to leucine and alanine: the first removed the aromatic character of phenyalanine, while maintaining the hydrophobic character, while the second eliminated both.

The affinities of the ligands for the WT and mutant receptors were determined on HEK-293 cells transiently transfected with MC4 receptor constructs. Receptor expression levels were determined by cell surface immunostaining and are shown in Table 2. All the mutants tested had expression levels similar to WT except I3.28(125) and F4.60(184) which in general showed lower expression.

NDP-α-MSH appeared to be a special case among all the ligands tested, since most of the mutants did not affect its binding affinity or functional activity (Tables 3 and 4). Only Y7.38(287)A and I7.42(291)A showed an effect on this ligand: Y7.38(287)A produced an 11-fold increase in binding K_i which is likely to be related to the 7.5-fold increase in its EC_{50} (Tables 3 and 4 and Figure 7); interestingly, the I7.42-(291)A mutation did not have any effect on the binding affinity of NDP-α-MSH but reduced dramatically ActMax (Table 6 and Figure 7).

The Y6.58(268)F and Y6.58(268)A Mutants. Y6.58(268) was predicted to be near the binding site, close to the loop region (Figure 6). According to our docking studies, the larger agonists, peptide **1** and α-MSH, were likely to have more extensive hydrophobic interactions with this locus than smaller ligands (Figure 6); we did not predict any specific hydrogen bond between this residue and any of the agonist or antagonist ligands used in the study. To test this hypothesis, we mutated this residue to phenylalanine and alanine and found that the response of the Y6.58(268)F construct to the different ligands was comparable to the WT receptor (Tables 3 and 4). This suggested that, as predicted, hydrogen bonding to this tyrosine was not important for binding or potency of any of our ligands. On the contrary, the alanine mutation had stronger effects on binding and efficacy: as is shown in Table 3, the Y6.58(268)A mutation had a strong effect in peptide agonist binding, with 23.4-fold increase in binding K_i for peptide **1** and 10.6-fold for α-MSH − with less consequences in compounds **3** and **4** binding (Table 3). The effect of these mutations on agonists potency followed the same trend as observed on binding Ki, with larger EC_{50} shifts observed for peptidic agonist (Table 4). Regarding antagonist binding, this mutation caused a 27.2 and 5.4-fold increase in the binding constants of peptide **2** and compound **5**, respectively (Table 3B) without affecting AGRP binding. The changes on antagonist IC_{50} were parallel to those observed in

Table 2. Cell Surface Expression of the MC4 WT and Mutant Receptors in Transiently Transfected HEK-293 Cells[a]

	% surface expression
MC4 WT	100 ± 0
Y268A	114 ± 7
Y268F	83 ± 4
Y287A	107 ± 8
Y287F	91 ± 6
F184A	90 ± 8
F184L	63 ± 5
I125A	51 ± 5
I129A	101 ± 10
I291A	101 ± 7

[a] Cell surface expression was measured by the 9E10 antibody binding directed against the c-myc-epitope inserted in the amino termini of WT and mutant constructs. The data are expressed as percent surface expression relative to WT expression level. Transfection efficiency of WT MC4R was typically 40% of transfected cells. The data are means ± SEM of a minimum of four experiments.

Table 3. Competitive Binding Affinities (K_is) of Agonist (A) and Antagonist (B) Compounds at Wild Type and Mutant MC4Rs[a]

(A) Agonist

	NDP-α-MSH		α-MSH		peptide **1**		compound **3**		compound **4**	
	K_i, nM	fold	K_i, nM	fold	K_i, nM	fold	K_i, nM	fold	K_i, nM	fold
MC4R WT	0.82 ± 0.09	1.0	22 ± 5	1.0	59 ± 5	1.0	6.7 ± 0.50	1.0	305 ± 88	1.0
Y268A	1.3 ± 0.22	1.6	231 ± 42	10.6	1370 ± 390	23.4	50 ± 14	7.6	1020 ± 110	3.3
Y268F	0.57 ± 0.16	0.7	25 ± 3	1.1	83 ± 4	1.4	4.6 ± 0.5	0.7	275 ± 100	0.9
Y287A	9.0 ± 4.0	11.0	257 ± 12	11.7	1490 ± 440	25.3	129 ± 28	19.4	2120 ± 1190	6.9
Y287F	0.97 ± 0.07	1.2	8.6 ± 0.9	0.4	90 ± 18	1.5	8.5 ± 1.9	1.3	890 ± 79	2.9
F184A	0.63 ± 0.02	0.8	9.3 ± 1.5	0.4	29 ± 1	0.5	3.2 ± 0.01	0.5	114 ± 10	0.4
F184L	0.56 ± 0.03	0.7	116 ± 30	5.3	407 ± 110	6.9	38 ± 9	5.8	1110 ± 360	3.6
I125A	1.2 ± 0.2	1.5	130 ± 6	5.9	111 ± 6	1.9	20 ± 5	3.1	1250 ± 530	4.1
I129A	0.63 ± 0.06	0.8	137 ± 8	6.2	710 ± 80	12.1	81 ± 7	12.2	3100 ± 570	10.2
I291A	0.63 ± 0.12	0.8	32 ± 5	1.4	173 ± 64	3.0	5.0 ± 1.3	0.8	260 ± 110	0.9

(B) Antagonist

	AGRP		peptide **2**		compound **5**	
	K_i, nM	fold	K_i, nM	fold	K_i, nM	fold
MC4R WT	1.8 ± 0.3	1.0	1.5 ± 0.4	1.0	160 ± 22	1.0
Y268A	3.2 ± 0.9	1.8	40 ± 11	27.2	870 ± 490	5.4
Y268F	1.1 ± 0.3	0.6	0.92 ± 0.12	0.6	151 ± 6	0.9
Y287A	6.1 ± 1.1	3.5	18 ± 0.8	12.0	2100 ± 1500	13.2
Y287F	1.8 ± 0.2	1.0	1.7 ± 0.6	1.1	560 ± 220	3.5
F184A	4.2 ± 0.03	2.4	0.71 ± 0.04	0.5	890 ± 500	5.5
F184L	23 ± 7	13.0	2.2 ± 0.3	1.5	1820 ± 270	11.3
I125A	1.3 ± 0.3	0.7	1.3 ± 0.3	0.9	120 ± 31	0.8
I129A	35 ± 8	20.1	14 ± 1	9.2	2990 ± 970	18.5
I291A	2.2 ± 0.6	1.2	3.2 ± 0.3	2.2	300 ± 35	1.9

[a] Competitive binding affinities are expressed as nM K_i. The data represent the mean ± SD of 2−3 experiments. Each experiment was performed in duplicate wells. Fold values compare binding of compounds to mutant receptor to that of wild-type receptor and are expressed as a ratio (mutant binding/wild-type binding).

Table 4. Potency (nM) of Agonist Compounds at Wild Type and Mutant MC4Rs[a]

	NDP-α-MSH		α-MSH		peptide **1**		compound **3**		compound **4**	
	EC_{50}	fold	EC_{50}	fold	EC_{50}	fold	EC_{50}	fold	EC_{50}	fold
WT	1.2 ± 0.2	1.0	2.9 ± 0.4	1.0	11 ± 2	1.0	1.2 ± 0.1	1	9.5 ± 3.0	1.0
Y268A	2.0 ± 0.8	1.7	21 ± 3	7.3	270 ± 50	25.3	0.82 ± 0.13	0.7	33 ± 3	3.5
Y268F	1.5 ± 0.2	1.2	7.1 ± 2.0	2.5	12 ± 3	1.2	1.5 ± 0.4	1.3	6.6 ± 2.2	0.7
Y287A	9.0 ± 2.0	7.5	156 ± 24	54.4	328 ± 54	30.7	26 ± 4	22.1	418 ± 87	44.2
Y287F	1.0 ± 0.2	0.9	2.6 ± 0.6	0.9	9.5 ± 2.1	0.9	0.61 ± 0.05	0.5	10 ± 3	1.1
F184A	0.51 ± 0.13	0.4	1.8 ± 0.4	0.6	3.2 ± 0.8	0.3	0.71 ± 0.2	0.6	1.02 ± 0.02	0.1
F184L	1.1 ± 0.3	1.0	18 ± 2	6.2	108 ± 15	10.1	8.5 ± 1.4	7.3	90 ± 2	9.5
I125A	1.4 ± 0.3	1.2	21 ± 3	7.2	202 ± 38	18.9	12 ± 2	10.0	53 ± 5	5.6
I129A	1.1 ± 0.2	0.9	27 ± 3	9.4	250 ± 53	23.3	41 ± 8	35.3	1520 ± 286	160.9
I291A	5.1 ± 2.5	4.2	89 ± 6	31.1	250 ± 64	23.4	$>10^3$		$>10^3$	

[a] Potency of agonist compounds was measured using cAMP accumulation assays. The data (nM EC_{50}) represent the mean ± SD of at least three experiments. Each experiment was performed in duplicate wells. Fold is relative to WT MC4R.

binding K_i: AGRP IC_{50} was not affected, peptide **2** IC_{50} showed a 15.7-fold increase in the IC_{50}, and compound **5** had a 4.8 increase in IC_{50} (Table 5, Figure 1 Supporting Information). It is worth noting that for all ligands, the changes on affinity and potency were of the same magnitude (Tables 3−5, Figure 1 Supporting Information), suggesting that the changes in ligand potency were a consequence of the changes in binding affinity, more than to a change in the efficacy of the receptor.

Y7.38(287)A and Y7.38(287)F Mutants. Y7.38(287) is aligned in rhodopsin with proline (Figure 3); during the refinement of the model, this locus of the helix was modeled as a straight helix. This refinement process lead to a repositioning of the Y738(287) side chain to the interior of the bundle. In this new orientation tyrosine presented not only a hydrophobic and aromatic surface to the binding site, but also introduced the capacity of a new hydrogen bond. Locus 7.38 is therefore a site of departure between the model and the template used to build it. If the reduction of the distortion at locus 7.38 was appropriate, and our hypothesis was correct, then mutation of this residue should affect ligand binding. If on the contrary this residue faces the phospholipid milieu, a lower effect (if any) would be expected. Following the same rational as in the Y6.58-(268) mutation, we mutated Y7.38(287) to F and A. The Y7.38-(287)A mutant affected the K_i of all the agonists tested between 25.3 (peptide 1) to 6.9-fold (compound 4) (Table 3A). It is noteworthy that this was the only mutation with significant effect on NDP-α-MSH, which showed an 11-fold increase in binding K_i (Table 3, Figure 7). The Y7.38(287)A mutation affected also the efficacy of all the ligands, with a maximum of 54.4-fold increase in α-MSH (Figure 2, A Supporting Information) to a minimum of 7.5-fold to NDP-α-MSH (Table 4, Figure 7). This mutation also affected antagonist binding, with changes in binding K_i between 13.2 and 3.5-fold (Table 3B). The magnitude of the changes in antagonists IC_{50}s was comparable to those shown in binding affinity, with an average shift of 6-fold (Table 5, Figure 2 Supporting Information).

The Y7.38(287)F mutation did not affect significantly the binding constant or the efficacy of any of the agonists or antagonist tested (Tables 3−5, Figure 2 Supporting Information), suggesting that the hydrogen bonding properties of Y7.38(287)

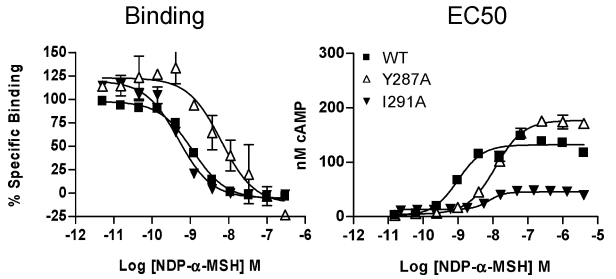

Figure 7. NDP-α-MSH binding and stimulation of cAMP in HEK-293 cells transiently expressing the wild type and the mutant receptors Y287A and I291A. For competition binding assays, the cells were incubated with 0.25 nM ^{125}I NDP-α-MSH and increasing concentrations of unlabeled NDP-α-MSH. For stimulation of cAMP accumulation, cells were incubated with 0.5 mM IBMX for 10 min followed by incubation with increasing concentrations NDP-α-MSH for 30 min at 37 °C. Graphs are representative figures of 2−5 experiments performed in duplicate wells with similar results.

Table 5. Inhibitory Activity (nM) of Antagonist Compounds at Wild Type and Mutant MC4Rs[a]

	AGRP (87−132)		peptide **2**		compound **5**	
	IC_{50}	fold	IC_{50}	fold	IC_{50}	fold
WT MC4R	40 ± 2	1.0	16 ± 3	1.0	560 ± 116	1.0
Y268A	40 ± 0.4	1.0	248 ± 24	15.7	2708 ± 157	4.8
Y268F	38 ± 0.3	1.0	17 ± 3	1.1	1030 ± 239.	1.8
Y287A	201 ± 19	5.0	121 ± 18	7.7	2900 ± 510	5.2
Y287F	31 ± 2	0.8	8.8 ± 0.7	0.6	355 ± 21	0.6
F184A	104 ± 7	2.6	11 ± 0.5	0.7	3770 ± 420	6.7
F184L	176 ± 5	4.4	18 ± 2	1.2	2860 ± 1520	5.1
I125A	11 ± 0.4	0.3	5.8 ± 1.0	0.4	160 ± 16	0.3
I129A	637 ± 55	15.9	131 ± 17	8.3	6190 ± 1400	11.1
I291A	18 ± 3	0.4	22 ± 5	1.4	708 ± 169	1.3

[a] Inhibitory activity of antagonist compounds was measured using cAMP accumulation assays. The data (nM EC_{50}) represent the mean ± SD of at least three experiments. Each experiment was performed in duplicate wells. Fold is relative to WT MC4R.

Table 6. Percent Efficacy of Agonist Compounds at Wild Type and Mutant MC4Rs[a]

	α-MSH	NDP-α-MSH	peptide **1**	compd **3**	compd **4**
WT MC4R	100 ± 0	89 ± 4	90 ± 7	110 ± 6	111 ± 17
Y268A	85 ± 5	83 ± 9	70 ± 5	104 ± 8	116 ± 3
Y268F	107 ± 5	96 ± 2	104 ± 9	111 ± 11	126 ± 15
Y287A	135 ± 8	128 ± 8	108 ± 9	132 ± 6	127 ± 16
Y287F	105 ± 8	104 ± 2	93 ± 9	118 ± 9	115 ± 10
F184A	86 ± 3	69 ± 7	76 ± 10	89 ± 9	89 ± 19
F184L	89 ± 7	87 ± 13	69 ± 4	99 ± 8	118 ± 9
I125A	87 ± 10	65 ± 17	33 ± 3	68 ± 5	102 ± 2
I129A	73 ± 4	77 ± 8	62 ± 3	79 ± 8	87 ± 2
I291A	25 ± 2	14 ± 1	11 ± 0	16 ± 5	25 ± 7

[a] Percent efficacy of agonist compounds was measured using cAMP accumulation assays. Data are normalized versus maximal response of α-MSH at WT MC4R. The data represent the mean ± SD of at least three experiments. Each experiment was performed in duplicate wells.

are not relevant for ligand binding. These results allowed us to rule out one of the poses obtained for compounds **3** and **4**, in which a hydrogen bond between Y7.38(287) and the carbonyl group in these two ligands appeared to be crucial to determine the orientation of the ligands in the binding site. These results suggest that this residue is likely to be part of a hydrophobic pocket shared by agonists and antagonists, without a clear distinction regarding the size of the molecule.

F4.60(184)A and F4.60(184)L Mutants. F4.60(184)A mutation did not affect significantly binding affinity (Table 3) or potency of any of the agonists tested (Table 4). The effect of this mutation on antagonists binding was minor (Table 3B) with

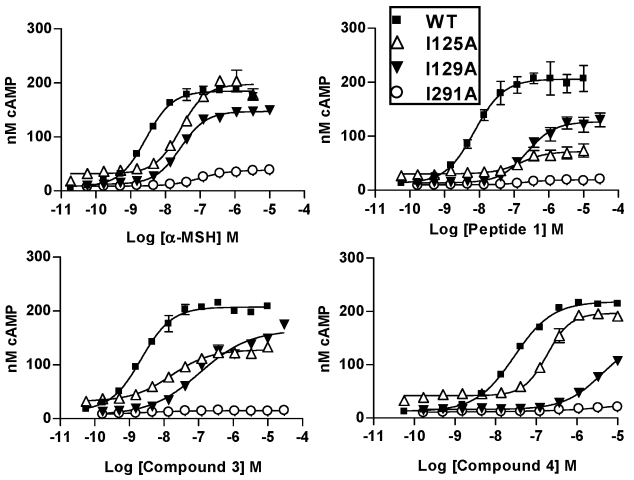

Figure 8. Stimulation of cAMP accumulation in HEK-293 cells transiently expressing the wild type and the mutant receptors I125A, I129A, I291A. Cells were incubated with 0.5 mM IBMX for 10 min followed by incubation with increasing concentrations α-MSH or compounds for 30 min at 37 °C. All panels are representative figures of 2−5 experiments performed in duplicate wells with similar results.

compound **5** showing the largest shift in K_i (5.5-fold increase) comparable with the 6.6-fold increase in its IC_{50} (Table 5, Figure 3G,H Supporting Information).

The leucine mutation (F4.60(184)L) had an average of 4-fold decrease in binding affinity with the exception of NDP-α-MSH, which was not affected. The effect of this mutation on agonists EC_{50} was comparable to the K_i increase, with an average of an 8-fold increase in EC_{50} (Table 4, Figure 3 Supporting Information), with the exception of NDP-α-MSH which, again, is not affected. The antagonists binding constants increased an average of 12-fold, (13-fold for AGRP; 11.3-fold for compound **5**), with the exception of the decapeptide peptide **2** which was not affected (Table 3B). Antagonists IC_{50}s were affected slightly less than the binding Ki, with a maximum of 5.1-fold increase for compound **5**, with the exception of peptide **2** which, parallel to the K_i, was not affected (Table 5).

I3.28(125)A, I3.32(129)A, and I7.42(291)A Mutants. The I3.28(125)A mutant effect on agonist binding varied, ranging from 6-fold for α-MSH binding to little effect on peptide **1** or NDP-α-MSH (Table 3A, Figures 11 and 7). The changes on EC_{50} were in general slightly larger than the changes in binding K_i (Table 4, Figure 8), and no change to NDP-α-MSH was observed (1.2-fold ratio mutant/WT, Table 4). For most of the agonists, Act Max was reduced to an average of 71% of that of WT (Table 6, Figure 8), which is likely related to the lower expression level found for the I3.28(125)A mutant (Table 2). Antagonists binding was not affected by the I3.28(125)A mutation (Table 3B), although the IC_{50} improved slightly (Table 5). It is worth noting that the calculated surface expression for this mutant was only 50% of that of WT.

The I3.32(129)A mutation caused an increase of binding K_i for both agonists and antagonists, that ranges between 12.2 and 6.2-fold in the case of the agonists (Table 3A, Figure 4 Supporting Information), and between 20.1 and 9.2 for the antagonists (Table 3B, Figure 9). As most of the mutants reported so far, NDP-α-MSH binding K_i or EC_{50} were not affected by this mutation. With the exception of NDP-α-MSH, the changes in EC_{50}s were larger than those observed for binding K_i, this was the case of α-MSH, and compounds **3** and **4** for which the EC_{50}s increased 9.4, 35.3, and 160.9-fold, respectively. ActMax was reduced an average of 76% with respect of

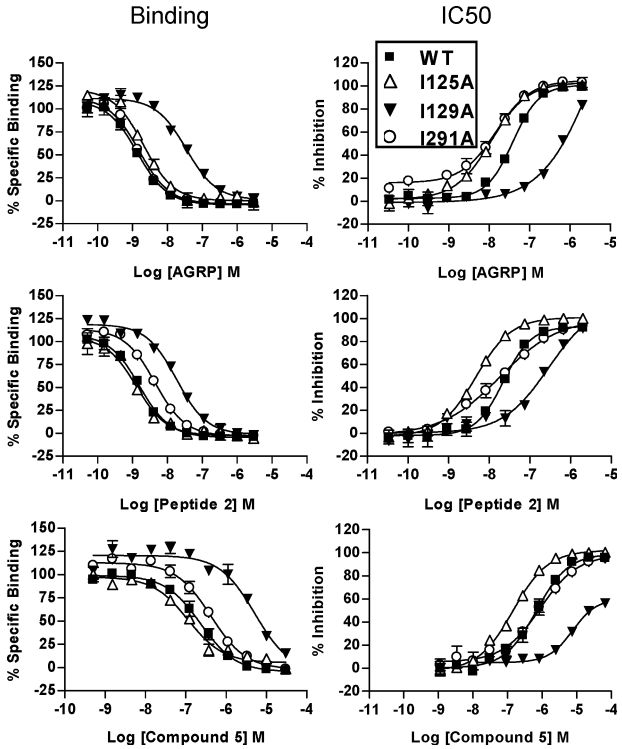

Figure 9. Antagonist binding (panels A, C, and E) and inhibition of cAMP accumulation (panels B, D, and F) in HEK-293 cells transiently expressing the wild type and the mutant receptors I125A, I129A, I291A. For competition binding assays the cells were incubated with 0.25 nM ^{125}I NDP-α-MSH and increasing concentrations of unlabeled compounds. For inhibition of cAMP accumulation, cells were incubated with 0.5 mM IBMX for 10 min followed by a 15 min preincubation with increasing concentrations compounds. NDP-α-MSH was then added at its EC_{50} concentration and cells were incubated for 30 min at 37 °C. All panels are representative figures of 2−5 experiments performed in duplicate wells with similar results.

WT (Figure 8, Table 6) which did not seem related to a change in receptor expression levels (Table 2). Antagonists IC_{50} also increased with a maximum of 15.9-fold change.

The I7.42(291)A mutant did not affect significantly agonists or antagonists binding affinity constants (Tables 3A,B, Figures 7 and 9, Figure 4 Supporting Information). For the three antagonists tested, this ratio was no higher than 2.2-fold as was the case of peptide **2**. On the contrary, the degree of maximum activation achieved by all the ligands tested in the I7.42(291)A mutant was severely decreased (Table 6, Figure 8). Interestingly, agonists and antagonists binding affinity as well as surface expression for this mutant were comparable to WT (Tables 2, 3A,B) and antagonists potency was preserved, which clearly suggests that the strong effect of this mutation on the efficacy of agonists was not the consequence of a grossly distorted mutant receptor but was most likely the result of a deficient activation mechanism at the receptor level.

3. Effects of the Mutations on Basal Activity. Changes in agonist binding affinity upon mutation of a residue in the protein are not always attributable to direct ligand−receptor interactions but can also be associated with changes in the equilibrium between the different conformational states accessible to the receptor. One assessment of this equilibrium is the determination of the basal activity of the receptor. MC4R has been shown to have constitutive activity in vitro.[47] Forskolin has been shown to potentiate the constitutive activity of Gs-coupled receptors, making it a useful tool to assess the activation state of GPCRs.[48] Our functional experiments did not show dramatic changes in

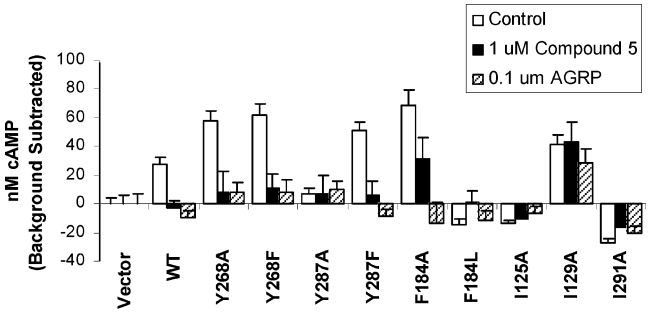

Figure 10. Basal activity of WT and mutant receptors was determined in forskolin stimulated HEK-293 cells treated with compound **5** (1 mM), AGRP (0.1 mM), or no treatment. Data shows fold stimulation of cAMP in receptor transfected cells over vector transfected cells. Figure is representative of four experiments performed in multiple wells all with similar results.

the initial c-AMP concentration measured before adding increasing concentration of agonists (Figures 7 and 8, Figures 1−3 Supporting Information). However, more subtle changes in basal activity can be detected by measuring cAMP accumulation on forskolin stimulated K293 transient transfectants. The adenlyate cyclase activity of MC4R WT receptor and several mutants (Y6.58(268)A, Y6.58(268)F, Y7.38(287)F, F4.60(184)A) was induced by stimulation with 10 μM of Forskolin (Figure 10). This activity was inhibited in the presence of the inverse agonist AGRP and the antagonist compound compound **5**, which therefore are inverse agonists. The largest increase in basal activity was observed for the F4.60(184)A mutant, which interestingly showed a slight tendency toward a lower agonists binding affinity values (Table 3A). This mutant showed also a slight decrease in antagonist affinity (Table 3B) (higher K_i), which might indicate that the effect of this mutation on ligand binding is likely to be the consequence of a change on the equilibrium between ground (R) and activated state of the receptor (R*). The higher population of R* is likely to account for the slight decrease on the agonists K_i value and the increase on antagonist K_i. With the exception of the mentioned F184A, and despite the increased basal activity, none of the mutants produced an increase in agonists binding affinities, suggesting that in those cases, it is more reasonable to assume a direct agonist-receptor interaction.

The I3.32(129)A mutant had a basal activity level very similar to WT when increasing amounts of forskolin were added; however, the basal activity was not reduced upon addition of the inverse agonist tested (data not shown and Figure 10). I3.29-(125)A, I7.42(291)A, and F4.60(184)L showed lower basal activity levels at all forskolin concentrations tested (data not shown and Figure 10). The lower basal activity of I3.29(125)A and F4.60(184)L may be due to lower surface expression relative to WT (Table 2); however, I7.42(291)A showed expression levels comparable to WT. We have shown above that the I7.42-(291)A mutant was less efficacious than the WT, while maintaining surface expression and ligand binding affinity. We observed that this mutant had the greater decrease in basal activity (Figure 10), as expected of a less efficacious receptor, although this reduction in basal activity did not affect agonist binding, which is maintained across the panel of agonists tested.

Discussion

The role of the MC4 receptor on the control of the feeding behavior makes it an attractive target for therapeutic intervention for the treatment of eating disorders. The present study attempts to understand the molecular mechanism of agonist binding and

activation in a structural context and to use that information in a structure-based drug design project of novel MC4 agonists. We used a double approach consisting of the use of a homology model of the MC4R to dock the ligands and the use of site-directed mutagenesis designed to test the hypothesis enumerated by the study of the molecular complexes. The model represents an activated state of the MC4R and includes a concerted rearrangement of the aromatic cluster in TM6[42,43] and the subsequent reduction of the kink at P6.50, resulting in the separation of the cytoplasmic ends of TM3 and TM6 shown to be crucial in the triggering of the activation signal in GPCRs.[38−40] To our knowledge, this model represents the first attempt to describe the MC4R in its active state.

A number of studies have made use of homology models based on rhodopsin together with site-directed mutagenesis to determine some of the interactions between peptide agonists and the MC4 receptor, identifying a number of key contacts between peptide agonists and the MC4R. These contacts involve: i) an ionic interaction of Arg8 with at least one of the conserved acidic residues D3.25(122), D3.29(126) in TM3, and E100(2.60) in TM2,[21,46] ii) a hydrophobic interaction between Phe7 on the peptide and F6.52(262),[8] iii) a Zn^{2+}-mediated interaction between His7 and D3.29(126) or D3.25(122).[19,20] Our computational docking studies were filtered according to their consistency with the published experimental data regarding the main ligand−receptor contacts. In addition to the residues reported in the literature, the selected poses revealed that also residues Y6.58(268), Y7.38(287), I3.28(125), I3.32-(129), and I7.42(291) line the binding site of the MC4R agonists. To test the role of these residues in binding and to investigate the role of the particular physicochemical properties that each one bestows to the region of the space it covers, we have mutated all of them to selected amino acids so that the phenotype would reveal the nature of the interaction with the ligand. All the mutants were tested for binding, functional, and basal activity.

The levels of receptor expression for all the mutants were similar to WT except for F4.60(184)L and I3.28(125)A mutants which was 63 and 51% of WT, respectively (Table 2). In addition to the low expression levels, the F4.60(184)L and I3.28-(125)A constructs also showed reduced levels of basal activity after forskolin stimulation. The I3.28(125)A mutation also produced a mild decrease in agonist binding and potency (Figure 8, Tables 3 and 4, Figure 4 Supporting Information) whereas antagonist binding and potency improved (Tables 3B, 5, Figure 9). This seems to indicate that I3.28(125) is likely to be part of the agonists binding site, and that it is not shared between agonists and antagonists binding sites. The weaker agonist binding may be the consequence of two synergistic processes: i) the loss of a contact binding interaction with the receptor and ii) a reduced population of receptors in R* in basal conditions. Concurrently an increase in antagonist affinity and potency might be related to a rise in the population of receptors in the ground state. The lower expression level of I3.28(125)A may account in part for the lower E_{max} observed for this mutant (Figure 8). The F4.60(184)L construct, having lower level of basal activity, caused a moderate loss in binding and efficacy for both agonists and antagonists (Tables 3A and 3B) suggesting that an aromatic residue at this locus provides a favorable interaction for both types of ligands, or that the presence of a bulky nonaromatic residue is unfavorable for both types of ligands.

The Y6.58(268)F and Y7.38(287)F mutations showed that the hydrogen bonding properties of tyrosine at these positions play a minor role in binding or activity of any of the ligands tested, since mutation of both residues to phenylalanine produced little effect on their binding and activation efficacy. Residue Y6.58(268) was predicted to lie on the most extracellular part of TM6, in the helical turn bordering the third extracellular loop. Our model predicted that Y6.58(268) has larger contacts with the larger ligands, mainly peptides, that can extend higher up than smaller agonist ligands (Figure 6) and therefore would be less affected by mutation of the residue. This hypothesis was confirmed by mutation of Y6.58(268) to alanine, which, as predicted, had a stronger effect over peptide binding and efficacy than for small molecules (Tables 3A,B and 4). The magnitude of the change in efficacy of agonists and antagonists was similar to the change on binding affinity, suggesting that the decrease in efficacy was only the consequence of a poorer binding. It has to be noted that at similar expression level as WT, Y6.58-(268)A mutation had an increased basal activity which confirms that the effect on the mutation of binding and efficacy is not the result of a change in the population of R versus R* but the result of a lost contact with the ligand.

The Y7.38(287)A mutant was characterized by a decrease in agonists binding affinity accompanied by a larger decrease in potency, suggesting that this residue is not only involved in a direct contact with the ligand but also on the transmission of the agonist signal. The shift in antagonist IC_{50} was of the same magnitude as the one in K_i, suggesting that the lost potency of antagonists is only the consequence of weaker binding. The basal activity of this mutant was decreased and antagonists failed to revert the basal level (Figure 10). It is worth noting that this locus is one of the points of departure between our model and the bovine rhodopsin crystal structure, since in rhodopsin this position is occupied by proline. The modification we introduced at this level, repositioned Y7.38(287) to face the binding site, is supported by the suggested involvement of this residue in direct contacts with the ligands.

Four residues downstream from Y7.38(287) in TM7, and therefore on the same face of the helix, we found that I7.42-(291) defined the base of a hydrophobic pocket where both peptidic and nonpeptidic agonists were likely to interact. This residue is positioned on top of the conserved "NPXXY motif", which has been shown to play an important role in receptor activation on a number of GPCRs such as rhodopsin,[49] 5HT2A,[50] and GNRH[18] among others and thus seems strategically positioned to transmit the activation signal from the binding site to the cytoplasmic part of the receptor, where the interaction with the G-protein occurs. The expression level of the I7.42-(291)A construct was comparable to WT (Table 2). Remarkably, agonist binding was unaffected by this mutation (Table 3A, Figure 4 Supporting Information), whereas the efficacy was dramatically reduced (Figure 8), indicating that I7.42(291) is a crucial residue involved in the activation mechanism of the receptor. As expected, this mutation produced the largest decrease in basal activity among the constructs tested (Figure 10). This construct displays an uncommon behavior, where a decreased basal activity did not affect ligand binding, but the efficiency of the receptor in transmitting the activation signal was severely impaired. These results are consistent with the proposed binding mode which suggests that agonists need to contact I7.42(291) to activate the receptor (in the case of peptides, by means of the tryptophan, in the case of compounds **3** and **4** through the cyclohexane (Figures 4B, 5B and 5D)), although this contact does not contribute to the binding energy. Therefore I7.42(291) and perhaps Y7.38(287) are likely to behave as another conformational switch that triggers and

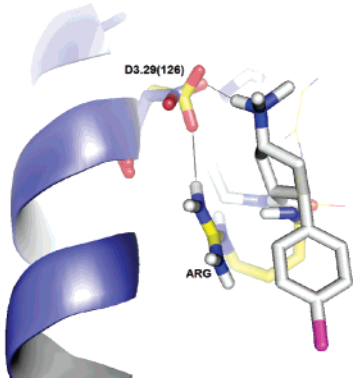

Figure 11. Highlight view of the interactions that residue D3.29(126) can achieve with the positive nitrogen of compound **4** (carbon atoms in white) and the arginine of the peptide (carbon atoms in yellow). The positive charge of compound **4** and peptide agonist do not overlap in space, but they are able to interact with the same residue in the protein.

transmits the activation signal to the intracellular side, likely through a conformational rearrangement of the "NPXXY" motif, two turns of a helix downstream, on the same face of the helix.

The proposed binding mode indicated that the basic amine of the small ligands interacts with D3.29(126), in a similar way to the arginine of the His-DPhe-Arg-Trp, although these positive charges do not overlap in space (Figure 11). The flexibility of the aspartic acid at 3.29 allows it to accommodate an interaction with a positive charge in slightly different positions in space. The peptide agonists have an additional interaction with the histidine of the His-DPhe-Arg-Trp message sequence (Figure 4) which might be mediated by Zn^{2+}.[19,20] The D-Phe of the peptides and the chlorophenyl group of small molecules interact with the aromatic cluster in TM6 when it is in an "active" conformation (Figures 4A, 5A and 5C), and last, the tryptophan of the peptides and the cyclohexane of small molecules fit in a hydrophobic pocket formed by I3.28(125), I3.32(129), and I7.42(291) (Figures 4B, 5B and 5D). Our model suggests that the basic amine of small molecule agonists points toward a flexible and less tight region occupied by the receptor loops, and therefore, larger substitutions of the positive nitrogen are likely to be tolerated. We also predicted that the chlorophenyl moiety fits in a tight aromatic region, suggesting that the aromatic character of the moiety is important and that only very small substitutions of the phenyl group might be tolerated. Synthesis of small molecule agonists designed along these lines allowed us to confirm these hypotheses (data not shown). An overlap of peptide 1 and compound **4** on the proposed pharmacophore is shown in Figure 6B.

In summary we have developed the first model of the MC4R in its activated state. Docking of agonists together with site-directed mutagenesis has identified important agonist-receptor interactions that provide a three-dimensional description of the pharmacophoric elements important for agonist binding. The agonist binding mode proposed provides a mechanistic explanation for the agonistic properties of the ligands studied and is consistent with all the previous literature reported in the past. We have identified a new hydrophobic and aliphatic pocket formed by I3.28(125), I3.32(129), and I7.42(291), which plays a crucial role in the activation mechanism of the MC4R. These results help shed light on the mechanism for MC4R agonism and should help guide the structure-based drug design of molecules with the capacity to modulate MC4R activity as potential therapeutics.

Acknowledgment. We thank Harel Weinstein, May Han, and David Yowe for helpful discussions.

Supporting Information Available: This material is available free of charge via the Internet at http://pubs.acs.org.

References

(1) Butler, A. A.; Cone, R. D. Knockout studies defining different roles for melanocortin receptors in energy homeostasis. *Ann. N. Y. Acad. Sci.* **2003**, *994*, 240−245.
(2) Farooqi, I. S.; Keogh, J. M.; Yeo, G. S.; Lank, E. J.; Cheetham, T. et al. Clinical spectrum of obesity and mutations in the melanocortin 4 receptor gene. *N. Engl. J. Med.* **2003**, *348*, 1085−1095.
(3) Nijenhuis, W. A.; Garner, K. M.; van Rozen, R. J.; Adan, R. A. Poor cell surface expression of human melanocortin-4 receptor mutations associated with obesity. *J. Biol. Chem.* **2003**, *278*, 22939−22945.
(4) Lubrano-Berthelier, C.; Cavazos, M.; Dubern, B.; Shapiro, A.; Stunff, C. L. et al. Molecular genetics of human obesity-associated MC4R mutations. *Ann. N. Y. Acad. Sci.* **2003**, *994*, 49−57.
(5) Vaisse, C.; Clement, K.; Durand, E.; Hercberg, S.; Guy-Grand, B. et al. Melanocortin-4 receptor mutations are a frequent and heterogeneous cause of morbid obesity. *J. Clin. Invest.* **2000**, *106*, 253−262.
(6) Elias, C. F.; Lee, C.; Kelly, J.; Aschkenasi, C.; Ahima, R. S. et al. Leptin activates hypothalamic CART neurons projecting to the spinal cord. *Neuron* **1998**, *21*, 1375−1385.
(7) Adan, R. A.; Hillebrand, J. J.; De Rijke, C.; Nijenhuis, W.; Vink, T. et al. Melanocortin system and eating disorders. *Ann. N. Y. Acad. Sci.* **2003**, *994*, 267−274.
(8) Haskell-Luevano, C.; Cone, R. D.; Monck, E. K.; Wan, Y. P. Structure activity studies of the melanocortin-4 receptor by in vitro mutagenesis: identification of agouti-related protein (AGRP), melanocortin agonist and synthetic peptide antagonist interaction determinants. *Biochemistry* **2001**, *40*, 6164−6179.
(9) Li, S. Z.; Lee, J. H.; Lee, W.; Yoon, C. J.; Baik, J. H. et al. Type I beta-turn conformation is important for biological activity of the melanocyte-stimulating hormone analogues. *Eur. J. Biochem.* **1999**, *265*, 430−440.
(10) Desai, P.; Prachand, M.; Coutinho, E.; Saran, A.; Bodi, J. et al. Activity and conformation of a cyclic heptapeptide possessing the message sequence His-Phe-Arg-Trp of alpha-melanotropin. *Int. J. Biol. Macromol.* **2002**, *30*, 187−195.
(11) Bondebjerg, J.; Xiang, Z.; Bauzo, R. M.; Haskell-Luevano, C.; Meldal, M. A solid-phase approach to mouse melanocortin receptor agonists derived from a novel thioether cyclized peptidomimetic scaffold. *J. Am. Chem. Soc.* **2002**, *124*, 11046−11055.
(12) Sebhat, I. K.; Martin, W. J.; Ye, Z.; Barakat, K.; Mosley, R. T. et al. Design and pharmacology of N-[(3R)-1,2,3,4-tetrahydroisoquinolinium- 3-ylcarbonyl]-(1R)-1-(4-chlorobenzyl)- 2-[4-cyclohexyl-4-(1H-1,2,4-triazol- 1-ylmethyl)piperidin-1-yl]-2-oxoethylamine (1), a potent, selective, melanocortin subtype-4 receptor agonist. *J. Med. Chem.* **2002**, *45*, 4589−4593.
(13) Goulet, M. T. N.; Ravi, P.; Ujjainwalla, F.; Walsh, T. F.; Warner, D. Acylated piperidine derivatives, specifically 1-[(aminocycloalkyl)-carbonyl]piperidines, as melanocortin-4 receptor agonists, and their pharmaceutical compositions and therapeutic uses. PCT Int. Appl. WO 0267869 A2, 2002.
(14) Ebersole, B. J.; Visiers, I.; Weinstein, H.; Sealfon, S. C. Molecular basis of partial agonism: orientation of indoleamine ligands in the binding pocket of the human serotonin 5-HT2A receptor determines relative efficacy. *Mol. Pharmacol.* **2003**, *63*, 36−43.
(15) Huang, P.; Visiers, I.; Weinstein, H.; Liu-Chen, L. Y. The local environment at the cytoplasmic end of TM6 of the mu opioid receptor differs from those of rhodopsin and monoamine receptors: introduction of an ionic lock between the cytoplasmic ends of helices 3 and 6 by a L6.30(275)E mutation inactivates the mu opioid receptor and reduces the constitutive activity of its T6.34(279)K mutant. *Biochemistry* **2002**, *41*, 11972−11980.
(16) Ballesteros, J. A.; Jensen, A. D.; Liapakis, G.; Rasmussen, S. G.; Shi, L. et al. Activation of the beta 2-adrenergic receptor involves disruption of an ionic lock between the cytoplasmic ends of transmembrane segments 3 and 6. *J. Biol. Chem.* **2001**, *276*, 29171−29177.
(17) Simpson, M. M.; Ballesteros, J. A.; Chiappa, V.; Chen, J.; Suehiro, M. et al. Dopamine D4/D2 receptor selectivity is determined by A divergent aromatic microdomain contained within the second, third, and seventh membrane-spanning segments. *Mol. Pharmacol.* **1999**, *56*, 1116−1126.
(18) Flanagan, C. A.; Rodic, V.; Konvicka, K.; Yuen, T.; Chi, L. et al. Multiple interactions of the Asp(2.61(98)) side chain of the gonadotropin-releasing hormone receptor contribute differentially to ligand interaction. *Biochemistry* **2000**, *39*, 8133−8141.

(19) Holst, B.; Elling, C. E.; Schwartz, T. W. Metal ion-mediated agonism and agonist enhancement in melanocortin MC1 and MC4 receptors. *J. Biol. Chem.* **2002**, *277*, 47662−47670.
(20) Holst, B.; Schwartz, T. W. Molecular mechanism of agonism and inverse agonism in the melanocortin receptors: Zn(2+) as a structural and functional probe. *Ann. N. Y. Acad. Sci.* **2003**, *994*, 1−11.
(21) Yang, Y. K.; Fong, T. M.; Dickinson, C. J.; Mao, C.; Li, J. Y. et al. Molecular determinants of ligand binding to the human melanocortin-4 receptor. *Biochemistry* **2000**, *39*, 14900−14911.
(22) Bakshi, R. K. B.; Khaled, J.; Nargund, R. P.; Palucki, B. L.; Patchett, A. A.; Sebhat, I.; Ye, Z.; Van Der Ploeg, L. H. T. Preparation of piperidine amino acid derivatives as melanocortin-4 receptor agonists. US Patent 20020137664 A1, 2000.
(23) Vos, T. J.; Caracoti, A.; Che, J. L.; Dai, M.; Farrer, C. A. et al. Identification of 2-{2-[2-(5-bromo-2-methoxyphenyl)-ethyl]-3-fluorophenyl}-4,5-dihydro-1H-imidazole (ML00253764), a small molecule melanocortin 4 receptor antagonist that effectively reduces tumor-induced weight loss in a mouse model. *J. Med. Chem.* **2004**, *47*, 1602−1604.
(24) Venkatachalam, C. M. Stereochemical criteria for polypeptides and proteins. V. Conformation of a system of three linked peptide units. *Biopolymers* **1968**, *6*, 1425−1436.
(25) Gibbs, A. C.; Kondejewski, L. H.; Gronwald, W.; Nip, A. M.; Hodges, R. S. et al. Unusual beta-sheet periodicity in small cyclic peptides. *Nat. Struct. Biol.* **1998**, *5*, 284−288.
(26) Syud, F. A.; Espinosa, J. F.; Gellman, S. H. NMR-based quantification of b-sheet populations in aqueous solution through use of reference peptides for the folded and unfolded states. *J. Am. Chem. Soc.* **1999**, *121*, 11577−11578.
(27) Peluso, S.; Ruckle, T.; Lehmann, C.; Mutter, M.; Peggion, C. et al. Crystal structure of a synthetic cyclodecapeptide for template-assembled synthetic protein design. *ChemBioChem* **2001**, *2*, 432−437.
(28) Rose, G. D.; Gierasch, L. M.; Smith, J. A. Turns in peptides and proteins. *Adv. Protein Chem.* **1985**, *37*, 1−109.
(29) Struthers, M.; Ottessen, J. J.; Imperiali, B. Design and NMR analysis of a compact, independently folded bba motif. *Folding Des.* **1998**, *3*, 95−103.
(30) Hutchinson, E. G.; Sessions, R. B.; Thornton, J. M.; Woolfson, D. N. Determinant of strand register in antiparallel beta-sheets of proteins. *Protein Sci.* **1998**, *7*, 2287−2300.
(31) Ottesen, J. J.; Imperiali, B. Design of a discretely folded mini-protein motif with predominantly beta-structure. *Nature Struct. Biol.* **2001**, *8*, 535−539.
(32) Ballesteros, J. A.; Weinstein, H. Integrated methods for the construction of three-dimensional models and computational probing of structure−function relations in G protein-coupled receptors. *Methods Neurosci.* **1995**, *25*, 366−428.
(33) Palczewski, K.; Kumasaka, T.; Hori, T.; Behnke, C. A.; Motoshima, H. et al. Crystal structure of rhodopsin: A G protein-coupled receptor. *Science* **2000**, *289*, 739−745.
(34) Visiers, I.; Ballesteros, J. A.; Weinstein, H. Three-dimensional representations of G protein-coupled receptor structures and mechanisms. *Methods Enzymol.* **2002**, *343*, 329−371.
(35) Visiers, I.; Braunheim, B. B.; Weinstein, H. Prokink: a protocol for numerical evaluation of helix distortions by proline. *Protein Eng.* **2000**, *13*, 603−606.
(36) Lefkowitz, R. J.; Cotecchia, S.; Samama, P.; Costa, T. Constitutive activity of receptors coupled to guanine nucleotide regulatory proteins. *Trends Pharmacol. Sci.* **1993**, *14*, 303−307.
(37) Samama, P.; Cotecchia, S.; Costa, T.; Lefkowitz, R. J. A mutation-induced activated state of the beta 2-adrenergic receptor. Extending the ternary complex model. *J. Biol. Chem.* **1993**, *268*, 4625−4636.
(38) Hubbell, W. L.; Cafiso, D. S.; Altenbach, C. Identifying conformational changes with site-directed spin labeling. *Nat. Struct. Biol.* **2000**, *7*, 735−739.
(39) Dunham, T. D.; Farrens, D. L. Conformational changes in rhodopsin. Movement of helix f detected by site-specific chemical labeling and fluorescence spectroscopy. *J. Biol. Chem.* **1999**, *274*, 1683−1690.
(40) Farrens, D. L.; Altenbach, C.; Yang, K.; Hubbell, W. L.; Khorana, H. G. Requirement of rigid-body motion of transmembrane helices for light activation of rhodopsin. *Science* **1996**, *274*, 768−770.
(41) Ghanouni, P.; Steenhuis, J. J.; Farrens, D. L.; Kobilka, B. K. Agonist-induced conformational changes in the G-protein-coupling domain of the beta 2 adrenergic receptor. *Proc. Natl. Acad. Sci. U. S. A.* **2001**, *98*, 5997−6002.
(42) Lin, S. W.; Sakmar, T. P. Specific tryptophan UV-absorbance changes are probes of the transition of rhodopsin to its active state. *Biochemistry* **1996**, *35*, 11149−11159.
(43) Filizola, M.; Visiers, I.; Skrabanek, L.; Campagne, F.; Weinstein, H. Functional mechanisms of GPCRs in a structural context. *Strategies in Molecular Neuropharmacology*; Humana Press: Totowa, NJ, 2003.
(44) Brooks, B. R.; Bruccoleri, R. E.; Olafson, B. D.; States, D. J.; Swaminathan, S. et al. CHARMM: a program for macromolecular energy, minimization, and dynamics calculations. *J. Comput. Chem.* **1983**, *4*, 187−217.
(45) McMartin, C.; Bohacek, R. S. QXP: powerful, rapid computer algorithms for structure-based drug design. *J. Comput.-Aided Molecular Des.* **1997**, *11*, 333−344.
(46) Yang, Y.; Dickinson, C.; Haskell-Luevano, C.; Gantz, I. Molecular basis for the interaction of [Nle4,D-Phe7]melanocyte stimulating hormone with the human melanocortin-1 receptor. *J. Biol. Chem.* **1997**, *272*, 23000−23010.
(47) Haskell-Luevano, C.; Monck, E. K. Agouti-related protein functions as an inverse agonist at a constitutively active brain melanocortin-4 receptor. *Regul. Pept.* **2001**, *99*, 1−7.
(48) Alewijnse, A. E.; Smit, M. J.; Rodriguez Pena, M. S.; Verzijl, D.; Timmerman, H. et al. Modulation of forskolin-mediated adenylyl cyclase activation by constitutively active G(S)-coupled receptors. *FEBS Lett.* **1997**, *419*, 171−174.
(49) Fritze, O.; Filipek, S.; Kuksa, V.; Palczewski, K.; Hofmann, K. P. et al. Role of the conserved NPxxY(x)5, 6F motif in the rhodopsin ground state and during activation. *Proc. Natl. Acad. Sci. U. S. A.* **2003**, *100*, 2290−2295.
(50) Konvicka, K.; Guarnieri, F.; Ballesteros, J. A.; Weinstein, H. A proposed structure for transmembrane segment 7 of G protein-coupled receptors incorporating an asn-Pro/Asp-Pro motif. *Biophys. J.* **1998**, *75*, 601−611.

JM050780S